Assorted Graphene-Based Nanofluid Flows Near a Reversed Stagnation Point over an Inclined Permeable Cylinder

Ghani, S. N.A.; Yarmand, Hooman; Noor, N. F.M.

DOI
10.1007/s40010-022-00782-z

Publication date
2022

Document Version
Final published version

Published in
Proceedings of the National Academy of Sciences India Section A - Physical Sciences

Proc. Natl. Acad. Sci., India, Sect. A Phys. Sci.
https://doi.org/10.1007/s40010-022-00782-z

SCIENTIFIC RESEARCH PAPER

Assorted Graphene-Based Nanofluid Flows Near a Reversed Stagnation Point over an Inclined Permeable Cylinder

S. N. A. Ghani[1] · Hooman Yarmand[2] · N. F. M. Noor[1,3]

Received: 13 August 2020 / Revised: 16 March 2022 / Accepted: 21 March 2022

Abstract Heat flux enhancement resulting from utilization of variant graphene-based nanoparticles; graphenes, graphene nanoplatelets, graphene oxides (GOs), carbon nanotubes (CNTs which include single and multiple walled CNTs) in a water-base fluid is focussed in the present study. A steady, laminar, incompressible, mixed convective and reversed stagnation point flow together with the consideration of transverse magnetic field over varying angles of an inclined permeable cylinder is analyzed for the heterogeneous nanofluids. The governing partial differential equations based on Tiwari-Das model are reformulated into nonlinear ordinary differential equations by applying similarity expressions. A shooting procedure is opted to reformulate the equations into boundary value problems which are solved by employing a numerical finite difference code utilizing three-stage Lobatto IIIa formula in MATLAB. The effects of constructive parameters toward the model on non-dimensional velocity and temperature disseminations, reduced skin friction coefficient and reduced Nusselt number are graphically reported and discussed in details. It is observed that GOs-water has the lowest heat flux performance under increasing values of wall permeability parameter, curvature parameter and nanoparticle volume fraction as compared to other nanofluids. On contrary, our results demonstrate that graphenes-water has the highest heat flux performance as compared to SWCNTs-water across many emerging parameters considered in this study.

Keywords Nanofluid · Tiwari-Das · Heterogeneous · Graphenes · GNPs · GOs

1 Research Relevance

Graphene is one of the nanoparticles with best heat transfer performance. Its unique thermal, electrical, optical and mechanical properties are very useful for many industrial utilizations since the material is stable, flexible, lightweight and sustainable. Due to these practical attractiveness, exploring the available variations of graphene-based nanoparticles is crucial since each combination of the nanofluids will have different heat flux performance hence different applications. The effects of varying angles of the inclined cylinder and the reversed stagnation point flow are also important as higher gradient of the surface promotes faster stream while reversed stagnation is relevant for the shear-thickening base fluids.

2 Introduction

Fluids play a major and significant duty for heat transfer in industrial processes such as transportation, cooling and heating exchangers, microelectronics and microfluidics, wire drawing, fuel cells, glass fiber, biomedical and pharmaceutical fields, food manufacturing and drug delivery. For that reason, a great deal of works in engineering,

✉ N. F. M. Noor
drfadiya@um.edu.my

[1] Institute of Mathematical Sciences, Faculty of Science, Universiti Malaya, 50603 Kuala Lumpur, Malaysia

[2] Department of Sustainable Design Engineering, Faculty of Industrial Design Engineering, Delft University of Technology, 2628 Delft, CE, The Netherlands

[3] Center for Data Analytics Consultancy and Services, Faculty of Science, Universiti Malaya, 50603 Kuala Lumpur, Malaysia

Published online: 26 May 2022

science and technology have been convened in this field to date. Despite that, the most frequently used base fluids, namely ethylene glycol, oil and water, limit the heat transfer analysis and effectiveness in consequence of their low thermal conductivity properties. Choi was the first who introduced the term nanofluid [1] to refer the combination of nano-scaled solid particles (nanoparticles) dispersed homogeneously into the base fluids to generate better heat transfer and energy power.

According to Haq et al. [2], nanoparticles tend to remain suspended a lot longer when compared to microparticles. Besides, the surface area per unit volume and the number of surface atoms per unit inside the nanoparticles are said to be much larger and higher than the microparticles [2]. With these characteristics, nanoparticles have the capabilities to reinforce the flow thermal conductivity, heat flux performance and other physical properties. Additionally, studies on nanoparticles in considerations of size, shape and type are also carried by the researchers for the purpose of measuring heat transfer efficiency of the fluid mixtures. Nanoparticles are made from different materials such as metal, oxide, carbide, carbon and functionalized nanoparticles. As a result, the research topic of nanofluids has been receiving increased attention worldwide. For example, Pandey et al. [3] reported in their studies that CuO and TiO2 nanofluids have the highest and the lowest heat transfer rates, respectively, while MgO nanofluid has the highest boundary layer thickness as compared to other hybrid nanofluids. Sheikholeslami et al. [4] examined a forced convection MHD heat transfer analysis of ferrofluid (Fe3O4-water) through a semi-annulus enclosed space. Verma et al. [5] analyzed the performance of Cu/Ag-H2O nanofluid in a diverging channel formed by two non-parallel walls past a Darcian porous medium and the outcome showed that the surface drag force and wall heat transfer rate for Cu-water nanofluid are stronger when compared with Ag-water nanofluid.

There are two different nanofluid models reported in the literature for heat transfer of boundary layer flows which are homogeneous and heterogeneous types. Hayat et al. [6] explained that the distinction is close to the fact that catalyst operates, respectively, in the same phase (gaseous phase) where the reaction takes place is said to be homogeneous or in different phase (solid phase) is said to be heterogeneous. These homogeneous and heterogeneous reaction parameters have opposite behaviors for different base fluids [6]. There are several researchers who operated on heat transfer and flow over a permeable surface by considering the heterogeneity of concentration due to crossed effect and other significant parameters. Bhattacharyya and Layek [7] examined boundary layer stagnation point flow over a porous shrinking sheet considering the effect of suction or blowing and radiation heat transfer in dual solutions. However, they claimed that heat transfer from the sheet increases by increasing the suction parameter, thermal radiation and Prandtl number for the first solution. Additionally, Seth et al. [8] studied the MHD stagnation point flow of an electrically conducting fluid and heat transfer past a non-isothermal shrinking/stretching sheet in a porous medium with presence of heat sink/source.

Moreover, a large number of numerical works have been conducted over the years to predict the heat transfer of nanofluid flows in diverse geometries and in different aspects. Kumar et al. [9] numerically uncovered that fluid mixtures with higher thermal conductivity and concentration contribute to huge effect on heat transfer when 0.75% CuO is added to the water base fluid. Bhattacharyya et al. [10] in their study perceived that the range of velocity ratio parameter of an incompressible fluid increases with increasing slip parameter. According to Selimefendigil et al. [11], the value of Nusselt number improves due to higher Richardson number when considering the elastic wall effect while Dinarvand et al. [12] discovered that the curvature parameter acts as one of the influential indicators in the inquiry of heat transfer for their selected metallic water-based nanofluid. In another extended study by Gholinia et al. [13], the concentrations and chemical species have been taken into consideration. Reddy et al. [14] found that the temperature profile enhances effectively with the nonlinear radiation as compared to linear radiation for the study of three-dimensional MHD slip flow of Eyring-Powell nanofluid flow over a slendering stretchable sheet. Ashorynejad et al. [15] demonstrated that greater magnitude of Darcy number results in higher permeability and heat transfer flow. The enhancement of heat transfer increases up to 32% for 0% to 0.1% concentration of graphene nanoparticles as noticed by Purbia et al. [16]. The research of Sheikholeslami et al. [17] confirmed that platelet shape of nanoparticles grants an outstanding impact on Nusselt number when compared with spherical shape of the nanoparticles. Apart from that, Haq et al. [18] mentioned that the suspension of solid CNTs within the common fluid-based engine oil gives the best rate of heat transfer and skin friction coefficient when compared with the rest of selected common fluids (water and ethylene glycol). Thus, from these literatures, it shows that the selection of nanoparticles in terms of type and shape together with type of common base fluids act as the significant factors in investigating thermal coefficient of the nanofluids.

The utilization of carbon-based nanoparticles in preparing nanofluid mixtures gives a considerable interest toward science and technological researchers. Even though SWCNTs and MWCNTs are known and broadly served as nanoparticles for high storage energy and better heat

transfer performance as compared to metallic nanoparticles, however, according to Kumar et al. [19], graphene as one of the carbon-based materials has also attracted a significant number of researchers to conduct scientific studies of its unique thermal, electrical, optical, mechanical and other relevant characteristics. Sadeghinezhad et al. [20] experimentally discovered that graphene has higher thermal conductivity than any other carbon-based nanoparticles. Additionally, Sadeghinezhad et al. [20] stated that graphene nanoparticles are more stable and have 1000 times larger surface area as compared to other nanoparticles. According to Ghozatloo et al. [21], thermal performance of graphene nanofluid in shell and tube heat exchanger is evidenced with the convection heat transfer coefficient has increased by 0.1 wt.% for graphene nanofluid.

Nevertheless, this study is the first attempt that examined graphenes, GNPs, GOs, SWCNTs and MWCNTs altogether in the heat transfer enhancement of heterogeneous nanofluids out of the long list of existing common literatures. The current research is also unique as it ventures on reversed stagnation point flow phenomenon which is rare with varying angles of the inclined permeable cylinder as the surface medium for heat exchanger. A finite difference code in MATLAB environment is utilized to solve the transformed boundary value problem from the initial set of governing partial differential equations defining the current variant graphene MHD nanofluids model. The enumerated results are validated and compared with previous published works of slightly different model of others by adjusting or dropping out some of the parameters presently foreseen. Emerging effects of constructive parameters toward the flow in terms of dimensionless velocity and temperature disseminations, skin friction coefficient and Nusselt number are simulated and discussed extensively. These findings are then presented in numerical tables and graphical disseminations for concluding remarks at the end.

3 Remarks on Governing Equations

This research considers a steady, laminar, incompressible, mixed convective and reverse stagnation point flow for selected mixtures of water-based nanofluids comprising variant graphene-based nanoparticles under the transverse magnetic field existence over an inclined permeable cylinder ω with radius R as shown in Fig. 1.

We let the wall surface temperature of the cylinder, T_w, and ambient temperature, T_∞, respectively, while assuming $U(x) = U_\infty(x/l)$ as the mainstream flow velocity. Uniform magnetic field of strength, B_0, and electrical conductivity, σ, are applied. Here, the cylindrical coordinates are opted

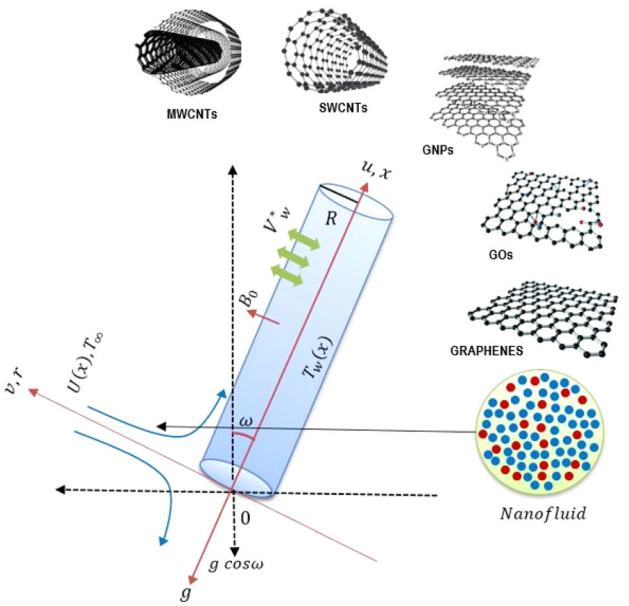

Fig. 1 Diagrammatic for the current problem with geometrical coordinates

in modelling the problems. Thereby, x-axis is positioned in assembling axial direction of cylinder whereas r-axis is perpendicular to the cylinder. Under these assumptions and following the proposed nanofluid model by Tiwari and Das [22], the relevant boundary layer equations can be defined as:

$$\frac{\partial u}{\partial x}(r) + \frac{\partial v}{\partial r}(r) = 0, \tag{1}$$

$$\frac{\partial u}{\partial x}(u) + \frac{\partial u}{\partial r}(v) = \frac{\partial U}{\partial x}U + v_{nf}\left(\frac{\partial^2 u}{\partial r^2} + \frac{\partial u}{\partial r}\frac{1}{r}\right) + \frac{\sigma {B_0}^2}{\rho_{nf}}(U-u) + \frac{\phi\rho_s\beta_s + (1-\phi)\rho_f\beta_f}{\rho_{nf}}g(T-T_\infty)cos\omega, \tag{2}$$

$$\frac{\partial T}{\partial x}(u) + \frac{\partial T}{\partial r}(v) = \alpha_{nf}\left(\frac{\partial^2 T}{\partial r^2} + \frac{\partial T}{\partial r}\frac{1}{r}\right). \tag{3}$$

The boundary conditions for the present problem are provided as follows:

$$u = 0, \quad v = V^*_w, \quad T = T_w(x) = T_\infty + \Delta T\left(\frac{x}{l}\right), \quad \text{at} \quad r = R,$$
$$u \to \kappa U(x), \quad T \to T_\infty, \quad \text{as} \quad r \to \infty, \tag{4}$$

where V^*_w is the uniform surface mass flux, in which two conditions of suction $V^*_w < 0$ and injection $V^*_w > 0$ should be considered. $\kappa > 0$ is denoted for positive stagnation flow and $\kappa < 0$ is implied for reversed stagnation flow as well as u and v are prescribed as the velocity components along the x and r directions. While T is the temperature for

the selected nanofluid, ϕ is the solid nanoparticle volume fraction, β_f, β_s, ρ_f and ρ_s are the thermal expansion coefficients and the densities of the selected base fluid and solid nanoparticles, respectively. Here, each of v_{nf} and α_{nf} are dedicated as the nanofluid kinematic viscosity and nanofluid thermal diffusivity, respectively, which are specified by Oztop and Abu-Nada [23]:

$$v_{nf} = \frac{\mu_f}{(1-\phi)^{2.5}[\phi\rho_s] + (1-\phi)\rho_f}, \tag{5}$$

$$\rho_{nf} = \left[\phi\rho_s + (1-\phi)\rho_f\right], \tag{6}$$

$$\alpha_{nf} = \frac{k_{nf}}{(\rho c_p)_{nf}}, \tag{7}$$

$$(\rho c_p)_{nf} = \phi(\rho c_p)_s + (1-\phi)(\rho c_p)_f, \tag{8}$$

$$\frac{k_{nf}}{k_f} = \frac{(k_s + 2k_f) - 2\phi(k_f - k_s)}{(k_s + 2k_f) + \phi(k_f - k_s)}, \tag{9}$$

in which k_{nf} indicates the nanofluid thermal conductivity, k_f and k_s are the thermal conductivities of the fluid and of the solid nanoparticles, respectively, while $c_{p_{nf}}$ denotes the nanofluid heat capacity, c_{p_f} and c_{p_s} are the heat capacities of the fluid and solid nanoparticles, respectively.

By initiating the given similarity transformations:

$$\eta = \frac{r^2 - a^2}{2v_f l}\sqrt{\frac{U_\infty v_f l}{a^2}}, \quad \psi = \sqrt{\frac{U_\infty v_f a^2}{l}}x\ddot{f}(\eta), \quad T = T_\infty + \Delta T\left(\frac{x}{l}\right)\ddot{\theta}(\eta), \tag{10}$$

where the stream function, ψ described in $u = r^{-1}\left(\frac{\partial\psi}{\partial r}\right)$ and $v = -r^{-1}\left(\frac{\partial\psi}{\partial r}\right)$, the continuity Eq. (1) will be fulfilled sufficiently as according to Haq et al. [12]. By substituting Eq. (10) into Eqs. (2) and (3), we obtain a system of dimensionless nonlinear ordinary differential equations as follows:

$$\frac{1}{(1-\phi)^{2.5}\left(\phi\frac{\rho_s}{\rho_f} + 1 - \phi\right)}\left[(1+2\gamma\eta)\ddot{f}''' + 2\gamma\ddot{f}''\right] + \frac{M}{\phi\frac{\rho_s}{\rho_f} + 1 - \phi}(1 - \ddot{f}') - \ddot{f}'^2 + \ddot{f}\ddot{f}'' + \frac{\phi\frac{\rho_s\beta_s}{\rho_f\beta_f} + 1 - \phi}{\phi\frac{\rho_s}{\rho_f} + 1 - \phi}\lambda\ddot{\theta}cos\omega = 0, \tag{11}$$

$$\frac{\frac{k_{nf}}{k_f}}{\phi\frac{(\rho c_p)_s}{(\rho c_p)_f} + 1 - \phi}\left[(1+2\gamma\eta)\ddot{\theta}'' + 2\gamma\ddot{\theta}'\right] + \Pr\left[\ddot{f}\ddot{\theta}' - \ddot{f}'\ddot{\theta}\right] = 0, \tag{12}$$

depending on the underlined boundary conditions:

$$\ddot{f}(0) = v_w, \quad \ddot{f}'(0) = 0, \quad \ddot{f}'(\infty) = \kappa, \quad \ddot{\theta}(0) = 1, \quad \ddot{\theta}(\infty) = 0, \tag{13}$$

where the primes express differentiation with respect to η, $\ddot{f}$ and $\ddot{\theta}$ are functions related to the dimensionless velocity field and temperature of the nanofluid, Pr is the Prandtl number, λ is the parameter for mixed convection, Gr is the Grashof number, Re is the Reynolds number, γ is the curvature parameter, v_w is the permeability parameter and M is the magnetic parameter which are all described mathematically as:

$$\Pr = \frac{c_p\mu_f}{k_f}, \quad \lambda = \frac{Gr}{Re^2}, \quad Gr = \frac{g\beta_f\Delta T l^3}{{v_f}^2}, \quad Re = \frac{U_\infty l}{v_f}, \quad \gamma = \sqrt{\frac{v_f l}{U_\infty^2}}, \quad v_w = -\frac{r}{a}\sqrt{\frac{l}{U_\infty v_f}}V^*_w, \quad M = \frac{\sigma {B_o}^2}{\rho_f\left(\frac{U_\infty}{l}\right)}. \tag{14}$$

Nonetheless, the mixed convection parameter λ corresponds to opposing flow when $\lambda < 0$ while $\lambda > 0$ corresponds to assisting flow. For the current concern, two essential physical properties which are the local skin friction coefficient, C_f, and the local Nusselt number, Nu, are described in mathematical expressions as follows:

$$C_f = \frac{\tau_w}{\rho_f {U_\infty}^2}, \quad Nu = \frac{lq_w}{\Delta T k_f}. \tag{15}$$

In above equations, τ_w and q_w are defined as shear stress and heat flux from the wall surface of the cylinder, respectively, which are denoted as:

$$\tau_w = \mu_{nf}\left(\frac{\partial u}{\partial r}\right)_{r=R} \quad \text{and} \quad q_w = -k_f\left(\frac{\partial T}{\partial r}\right)_{r=R}. \tag{16}$$

By invoking Eqs. (10), (15) and (16), the dimensionless forms can be obtained as follows:

$$Re^{\frac{1}{2}}C_f = \frac{\left(\frac{x}{l}\right)}{(1-\phi)^{2.5}}\ddot{f}''(0), \quad Re^{\frac{1}{2}}Nu = -\frac{k_{nf}}{k_f}\left(\frac{x}{l}\right)\ddot{\theta}'(0). \tag{17}$$

4 Methodology Toward Solution

An appropriate solution approach is compulsory to meet the accuracy of the outcomes for the current governing partial differential equations. The numerical solution for the present incompressible MHD reversed stagnation point flow of a viscous nanofluid concerning the mixed convection heat transfer is performed by using the MATLAB package (bvp4c). This numerical approach is inevitably simple, low cost but has high computational speed across many other computational procedures. The coding has been proven to be fruitful in producing adequate solutions for

numerous nonlinear mathematical and engineering problems.

The nonlinear ordinary differential Eqs. (11) and (12) under the boundary conditions (13) are reformulated by performing a shooting technique in this section. Then, the differential equations are decreased to first-order system in the following forms:

$$\ddot{f}'_{(3)} = -\frac{1}{1+2\gamma\eta}\left((1-\phi)^{2.5}\left(\phi\frac{\rho_s}{\rho_f}+1-\phi\right)\left[\ddot{f}_{(1)}\ddot{f}_{(3)}+1-(\ddot{f}_{(1)})^2,\right.\right.$$
$$\left.\left.+\frac{\phi\frac{\rho_s\beta_s}{\rho_f\beta_f}+1-\phi}{\phi\frac{\rho_s}{\rho_f}+1-\phi}\lambda\ddot{f}_{(4)}cos\omega+\frac{M}{\phi\frac{\rho_s}{\rho_f}+1-\phi}(1-\ddot{f}_{(2)})\right]+2\gamma\ddot{f}_{(3)}\right), \tag{18}$$

$$\ddot{f}'_{(5)} = -\frac{1}{1+2\gamma\eta}\left(\left(\frac{\phi\frac{(\rho c_p)_s}{(\rho c_p)_f}+1-\phi}{\frac{k_{nf}}{k_f}}\right)Pr[\ddot{f}_{(1)}\ddot{f}_{(5)}-\ddot{f}_{(2)}\ddot{f}_{(4)}]+2\gamma\ddot{f}_{(5)}\right), \tag{19}$$

with the following boundary conditions:

$$\ddot{f}_{(1)}(0)=v_w,\quad \ddot{f}_{(2)}(0)=0,\quad \ddot{f}_{(4)}(0)=1,\quad \ddot{f}_{(2)}(\infty)=\kappa,$$
$$\ddot{f}_{(4)}(\infty)=0, \tag{20}$$

by applying the following variables:

$$\ddot{f}=\ddot{f}_{(1)},\quad \ddot{f}'=\ddot{f}_{(2)}=\ddot{f}'_{(1)},\quad \ddot{f}''=\ddot{f}_{(3)}=\ddot{f}'_{(2)},\quad \ddot{f}'''=\ddot{f}'_{(3)},$$
$$\ddot{\theta}=\ddot{f}_{(4)},\quad \ddot{\theta}'=\ddot{f}_{(5)}=\ddot{f}'_{(4)},\quad \ddot{\theta}''=\ddot{f}'_{(5)}. \tag{21}$$

The selected limit for η is 14 and the initial values for $\ddot{f}_{(3)}$ and $\ddot{f}_{(5)}$ are assumed to be 0. The boundary value problem is further solved under the residual tolerance of 10^{-6}.

5 Analytical Insights

In this section, the outcomes of the boundary layer properties, namely non-dimensional velocity and temperature disseminations, local skin friction coefficient and Nusselt number, are carefully scrutinized for varying parameters. We consider five types of graphene-based nanoparticles: graphenes, GNPs, GOs, SWCNTs and MWCNTs. Thermophysical properties of these selected nanoparticles and the base fluid (water) are provided in Table 1. The values of solid nanoparticle volume fraction parameter, ϕ are simulated from 0 to 0.4 for this current problem. For the purpose of verification for the present study, we validated our results calculated via the present bvp4c code for water-based copper nanofluids (Cu-water) with the formerly reported results obtained by Dinarvand et al. [9] by using homotopy analysis method (HAM) and fourth-order Runge–Kutta method (RK4). The comparisons depicted in Table 2 demonstrate a very good agreement between our results and theirs.

Figs. 2, 3, 4, 5, 6 illustrate the effect of stagnation parameter κ, inclination angle ω, mixed convection parameter λ, Prandtl number Pr, curvature parameter γ, wall permeability parameter v_w, magnetic parameter M and solid nanoparticle volume fraction ϕ of the selected nanoparticles on the model's dimensionless velocity and temperature disseminations. Firstly, the behavior of stagnation parameter κ is depicted in Figs. 2a–c. Further, Figs. 2a, b explain that the velocity dissemination starts to rise near the surface of the cylinder and begins to fall off apart from the surface of the cylinder. The corresponding Fig. 2a shows that MWCNTs-water has the highest fluid velocity and the results for temperature dissemination almost similar for all nanofluids when $\kappa=-3$. For $\kappa=0$, there is no stagnation point that occurs in the streamline while the fluid velocity is strongly enhanced for all nanofluids when there is no stagnation point and positive stagnation $\kappa=3$ is imposed to the flow where the impact of SWCNTs on velocity profile is more prominent in this case (see Figs. 2b, c). Graphenes-water contributes to the least temperature dissemination in both corresponding stagnation problem. In general, the fluid temperature decreases for all cases of stagnation parameter κ. However, it is worth to emphasize that the thermal boundary layer thickness and temperature dissemination of GOs-water are more prominent at both $\kappa=0$ and $\kappa=3$.

The characteristics nature of inclination angle ω on velocity dissemination is visualized in Figs. 3a, b. Fluid velocity slightly reduces with the increase in ω. In fact, gravity effect is minimized for inclined cylinder $(0<\omega\leq 90)$ and it results in decreasing velocity

Table 1 Thermophysical properties of the base fluid (water) and selected graphene-based nanoparticles

Thermophysical properties	Water [12, 24]	SWCNTs [12, 24]	MWCNTs [12, 24]	Graphenes [25, 26]	GOs [27, 28]	GNPs [29]
k (W/mK)	0.613	6600	3000	2500	5000	3000
ρ (kg/m^3)	997.1	2600	1600	2250	1800	2200
C_p (J/kgK)	4179	425	796	2100	717	538.2

Table 2 Effects of solid nanoparticle volume fraction and mixed convection on both skin friction coefficient and Nusselt number for copper-water nanofluid when Pr=6.2, γ=1, M=0 and v_w=0

λ	ϕ	$(l/x)Re^{1/2}C_f$			$(l/x)Re^{1/2}Nu$		
		[4]		Present	[4]		Present
		HAM	RK4	bvp4c	HAM	RK4	bvp4c
0.0	0.0	1.70764	1.70762	1.70766	2.15177	2.15173	2.15175
	0.1	2.51216	2.51214	2.51213	2.69664	2.69666	2.69667
	0.2	3.46826	3.46828	3.46829	3.26935	3.26939	3.26938
1.0	0.0	1.99210	1.99215	1.99218	2.21366	2.21362	2.21363
	0.1	2.79276	2.79273	2.79271	2.74838	2.74831	2.74831
	0.2	3.75691	3.75698	3.75700	3.31539	3.31532	3.31533
5.0	0.0	3.02007	3.02004	3.02005	2.40937	2.40936	2.40935
	0.1	3.83616	3.83608	3.83609	2.92289	2.92285	2.92286
	0.2	4.84849	4.84840	4.84841	3.47660	3.47668	3.47668

dissemination [16]. As can be seen, the influence of SWCNTs-water (for the highest velocity dissemination) and graphenes-water (for the lowest temperature dissemination) are more eminent than other nanofluids when the inclination angle, ω, is increased from 0 up to 40 degrees (see Fig. 3b). Oppositely, MWCNTs-water consistently contributes toward the lowest velocity dissemination but the highest temperature dissemination when $0 \leq \omega \leq 40$.

The changes in the mixed convection parameter consisting assisting flow ($\lambda > 0$) and opposing flow ($\lambda < 0$) on velocity disseminations are portrayed in Figs. 4a, b. To be specific, Figs. 4a, b are sketched to show the motion trend of the nanofluids when $\lambda = -3$ and $\lambda = 3$. It is noted that the rise in λ decreases the fluid velocity. The result shows that graphenes-water dominates over the velocity dissemination for assisting flow when λ is increased to 3. Graphenes-water also produces the lowest temperature dissemination as compared to other nanofluids regardless the impact of assisting ($\lambda = 3$) or opposing flow ($\lambda = -3$).

Figs. 5a, b capture the trend of the fluid velocity for all selected nanofluids with variation of Prandtl number Pr. The velocity dissemination remains almost stagnant because Pr only appears in the energy Eq. (12). As depicted in Fig. 5a, it is important to mention that graphenes-water under low Prandtl number offers a positive impact on the flow speed as compared to other nanofluids. Again, graphenes-water gives the lowest temperature dissemination here than other nanofluids at any value of Pr. Figures 3, 4, 5 show that the fluid temperature declines faster for larger inclination angle ω, mixed convection λ and Pr values. In all these considered figures, graphenes-water emerges as the best nanofluid since it has the highest heat flux performance to maintain the flow at the minimum temperature as compared to other nanofluids. Additionally, it is worth to highlight that GOs-water contributes to the lowest flow velocity at a smaller value of Prandtl, Pr, but at a greater value of mixed convection λ.

The effects of curvature parameter γ, wall permeability parameter v_w, magnetic parameter M and solid nanoparticle volume fraction ϕ on velocity dissemination are presented in Figs. 6a–d. It is found that an increment in γ and ϕ results in the reduction of fluid velocity while increasing the fluid temperature. The rise of ϕ results in increasing nanofluid viscosity which then slows down the fluid motion. Furthermore, thermal conductivity and boundary layer thickness are enhanced as ϕ increases. Fluid velocity rises more rapidly for all selected nanofluids when M and v_w increase. However, increasing the value of M and v_w causes the temperature dissemination to decay for all nanofluids. Given that, by improving the value of M generates higher resistance force in the current and depresses the hydrodynamic boundary layer thickness, hence resulting to a slower flow, consequently decreases the fluid temperature as reported in [9]. In the current research, the suction case ($v_w > 0$) and the injection case ($v_w < 0$) are implemented. From all the considered figures, it is discovered that the velocity dissemination declines close to the wall surface of the cylinder while it increases apart from the cylinder. The opposite trend is noticed for temperature dissemination. A small gap of fluid velocity and temperature appears between all selected nanofluids due to differences in thermophysical properties of the nanofluids. The results in Figs. 6a, b present that the couple graphenes-water and SWCNTs-water both dominate over the velocity dissemination at $\gamma = 0.8$ and $v_w = 1$. On the other hand, Figs. 6c, d illustrate that graphenes-water still has the highest velocity dissemination after increasing the value of M and ϕ up to 8.0 and 0.4, respectively. Additionally, it is

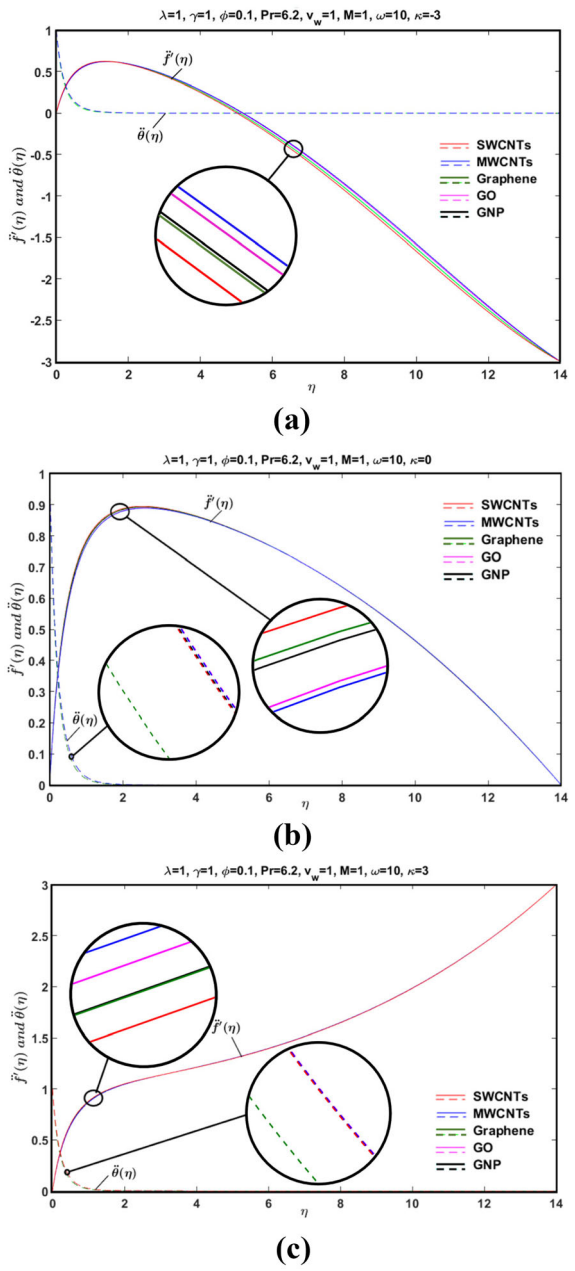

Fig. 2 Influence of stagnation parameter **a** $\kappa = -3$ (reversed stagnation), **b** $\kappa = 0$ (zero stagnation) and **c** $\kappa = 3$ (positive stagnation) on velocity and temperature disseminations for the nanofluids

examined that GOs-water contributes the most outstanding development of fluid temperature when increasing the value of v_w, γ and ϕ as compared to other selected nanofluids. This signifies that GOs-water has the lowest heat flux performance.

Figures 7 and 8 represent the impact of all emerging parameters for both skin friction coefficient and Nusselt number, respectively. It should be emphasized that the enhanced heat transfer rate and surface tension are owing to their correlation with skin friction coefficient and Nusselt number [9]. An increment in the curvature parameter γ, Hartmann number M, Prandtl number Pr and wall permeability parameter v_w result in enhancement of reduced skin friction coefficient (Figs. 7a–d) and Nusselt number (Figs. 8a–d). However, increasing the mixed convection λ value constantly decreases the skin friction coefficient and Nusselt number for all selected nanofluids (see Figs. 7e and 8e). Eventually, graphenes-water emerges as the most significant nanofluid with the highest rates of reduced skin friction coefficient (Figs. 7a–d for γ, M, Pr and v_w) and reduced Nusselt number (Figs. 8a–c, e, h for γ, M, Pr, λ and ω) against SWCNTs-water, MWCNTs-water, GNPs-water and GOs-water.

The effects of ϕ on skin friction coefficient and Nusselt number for all selected nanofluids are illustrated in Figs. 7f and 8f. The skin friction coefficient is gradually increases as ϕ increases. As can be viewed in Fig. 8f, it is pointed out that except for graphenes-water, the trend of reduced Nusselt number for the rest of the nanofluids decreases when ϕ increases up to 0.2. The trend however started to rise again from 0.2 to 0.4. It is important to emphasize that graphenes-water excellently dominates over the skin friction and Nusselt number when the nanoparticles volume concentration ϕ is increasing.

Furthermore, Figs. 7g and 8g indicate changes in skin friction coefficient when the value of stagnation parameter κ is raised. The studied figures show that GNPs-water and SWCNTs-water are more sensitive toward skin friction coefficient and Nusselt number when $\kappa < 0$ (reversed stagnation) while graphenes-water progressively dominates skin friction coefficient and Nusselt number when $\kappa > 0$ (positive stagnation). It is also notable that there is only a minor change in Nusselt number for all the nanofluids when $\kappa > 0$ (see Fig. 8g). Apart from that, Figs. 7h and 8h display the relationship between skin friction coefficient and Nusselt number versus the inclination angle ω. There is no particular pattern that can be sufficiently defined in reduced skin friction coefficient with respect to the inclination angle ω; however, the contrary result can be observed in Fig. 8h in which graphenes-water strongly dominates the reduced Nusselt number as compared to other nanofluids. Basically, this indicates that the high friction wall surface of the heat exchanger is obtained when the particles have larger density properties. In contrast, the specific heat capacity and thermal conductivity of nanofluids provide an influential contribution for heat transfer efficiency. On top of all these, it is also remarkable how graphenes-water easily beat off the performance of SWCNTs-water and other nanofluids across many emerging parameters considered in the current work.

A closer look on the numerical values addressed for each physical parameter of both reduced skin friction

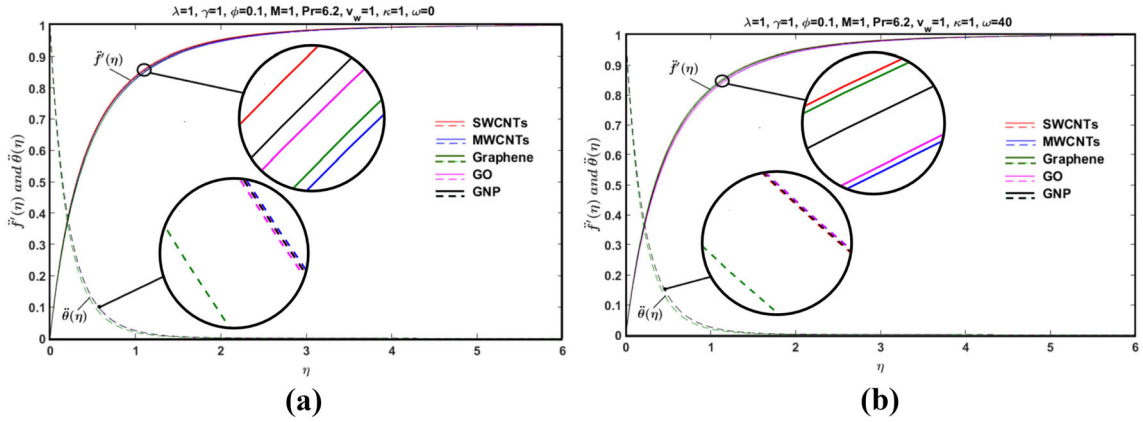

Fig. 3 Influence of inclination angle **a** $\omega = 0$ and **b** $\omega = 40$ on the velocity and temperature disseminations for the nanofluids

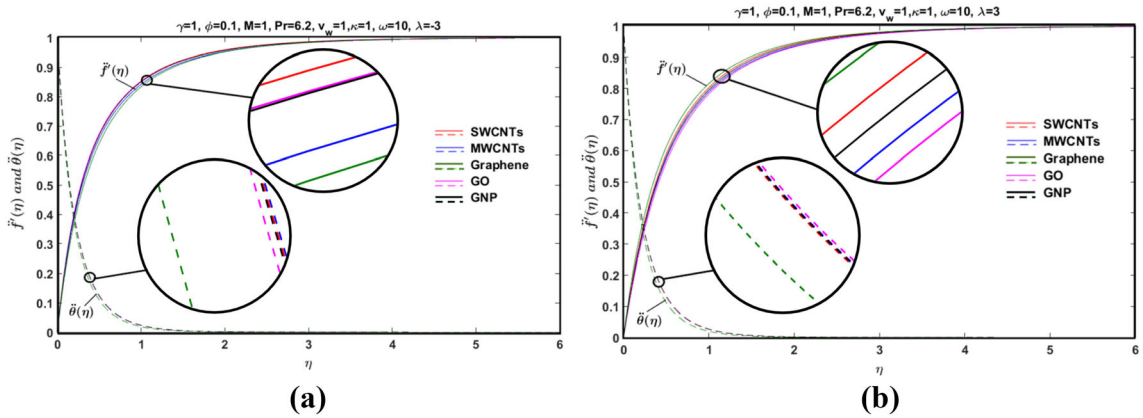

Fig. 4 Influence of mixed convection **a** $\lambda = -3$ and **b** $\lambda = 3$ on the velocity and temperature disseminations for the nanofluids

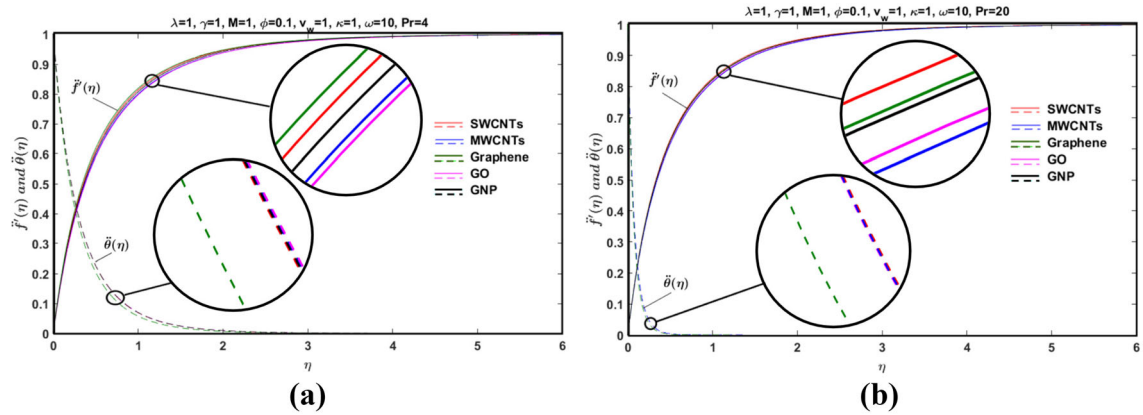

Fig. 5 Influence of Prandtl number **a** $Pr = 4$ and **b** $Pr = 20$ on the velocity and temperature disseminations for the nanofluids

coefficient and reduced Nusselt number to sustain the latter statement is possible as outlined in Table 3. It is obvious that graphenes-water has the highest heat flux performance as compared to other nanofluids considered based on its value of reduced Nusselt number.

6 Conclusive Remarks

In this study, a steady, laminar, incompressible, mixed convective and reversed stagnation point flow of heterogeneous graphene-based nanofluids flows in the existence

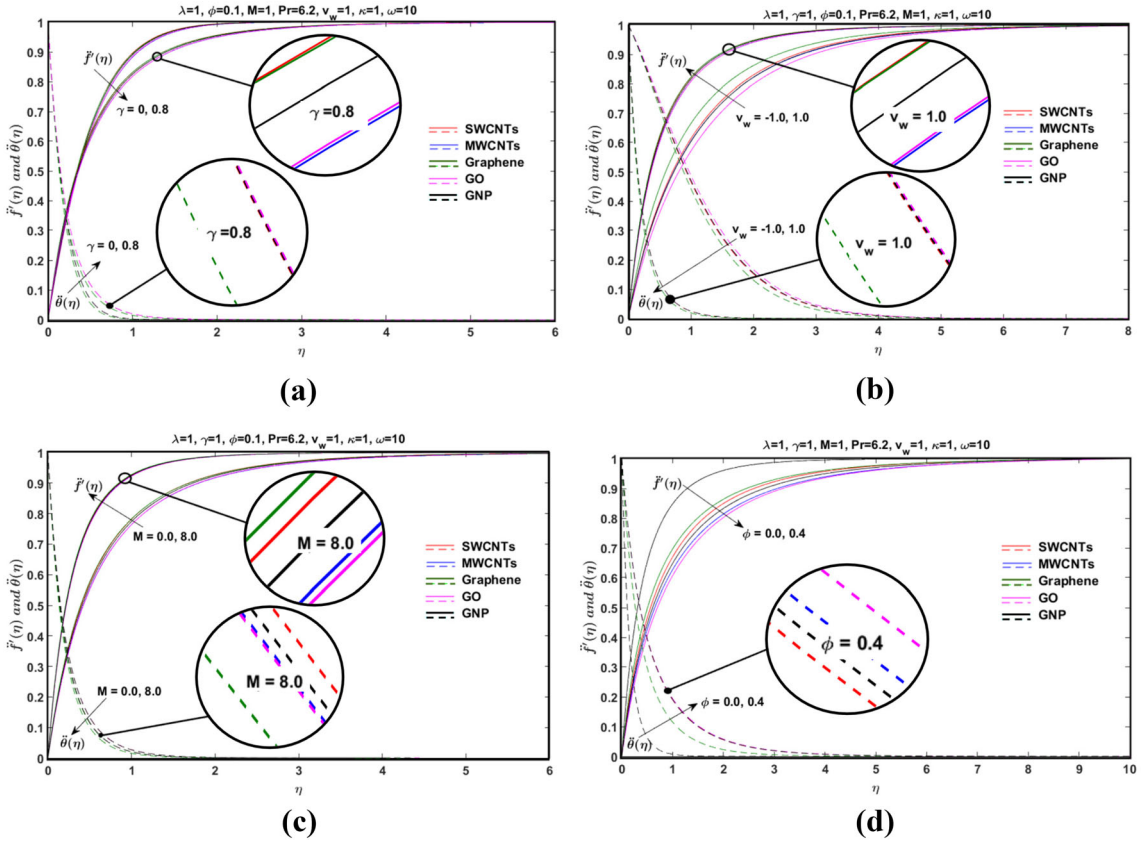

Fig. 6 The effect of **a** the curvature parameter, **b** the wall permeability parameter, **c** the magnetic parameter and **d** the solid nanoparticle volume fraction parameter on the velocity and temperature disseminations for the nanofluids

of transverse magnetic field past an inclined permeable cylinder has been examined. The governing partial differential equations were transformed to nonlinear ordinary differential equations by using similarity variables before they were solved numerically using bvp4c package in MATLAB.

The effects of emerging parameters on the heterogeneous flow for different nanoparticles: graphenes, GOs, GNPs, SWCNTs and MWCNTs with water as the base fluid are analyzed and discussed with aid of tables and figures. The following outcomes are deduced:

1. In general, graphenes-water has the highest skin friction and heat flux performance as compared to other nanofluids across many emerging parameters considered in this work.
2. GOs-water has the lowest heat flux performance under increasing values of wall permeability parameter, curvature parameter and nanoparticle volume fraction as compared to other nanofluids especially for zero and positive stagnation ($\kappa = 0, 3$).
3. Velocity dissemination decreases nearly to the wall cylinder surface and increases as the flow moves away from the cylinder for all nanofluids. The opposite trend is noticed for temperature dissemination.
4. SWCNTs-water has the highest velocity as ω increases from 0 to 40 degrees.
5. An increment in the curvature parameter, Prandtl number, Hartmann number and wall permeability parameter indicates the enhancement of skin friction coefficient and Nusselt number. However, increasing the value of mixed convection parameter constantly decreases the reduced skin friction coefficient and Nusselt number for all selected nanofluids.
6. GNPs-water and SWCNTs-water are more sensitive toward skin friction coefficient and Nusselt number in reversed stagnation flow.

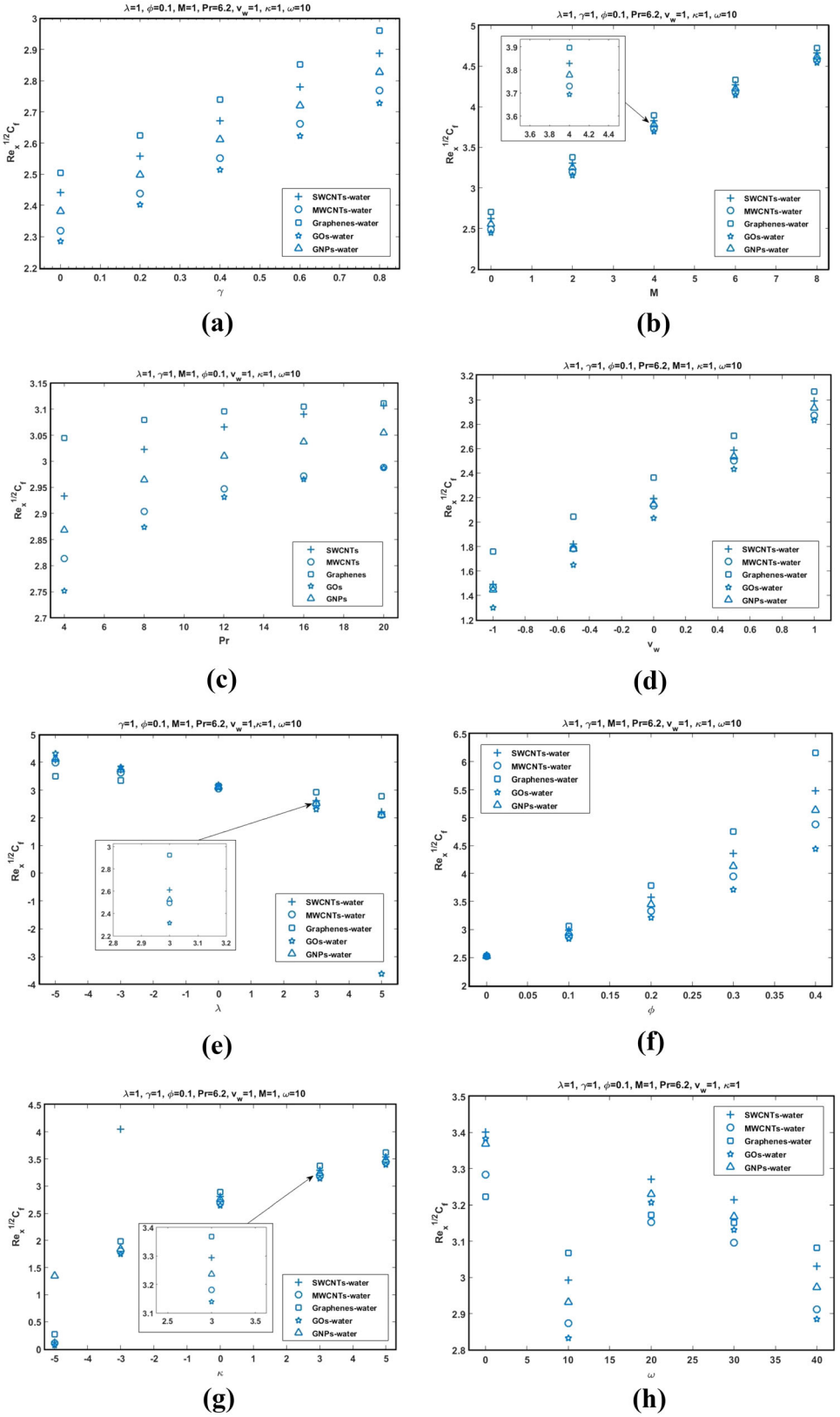

Fig. 7 Impacts of parameter variation on reduced skin friction coefficient for the nanofluids

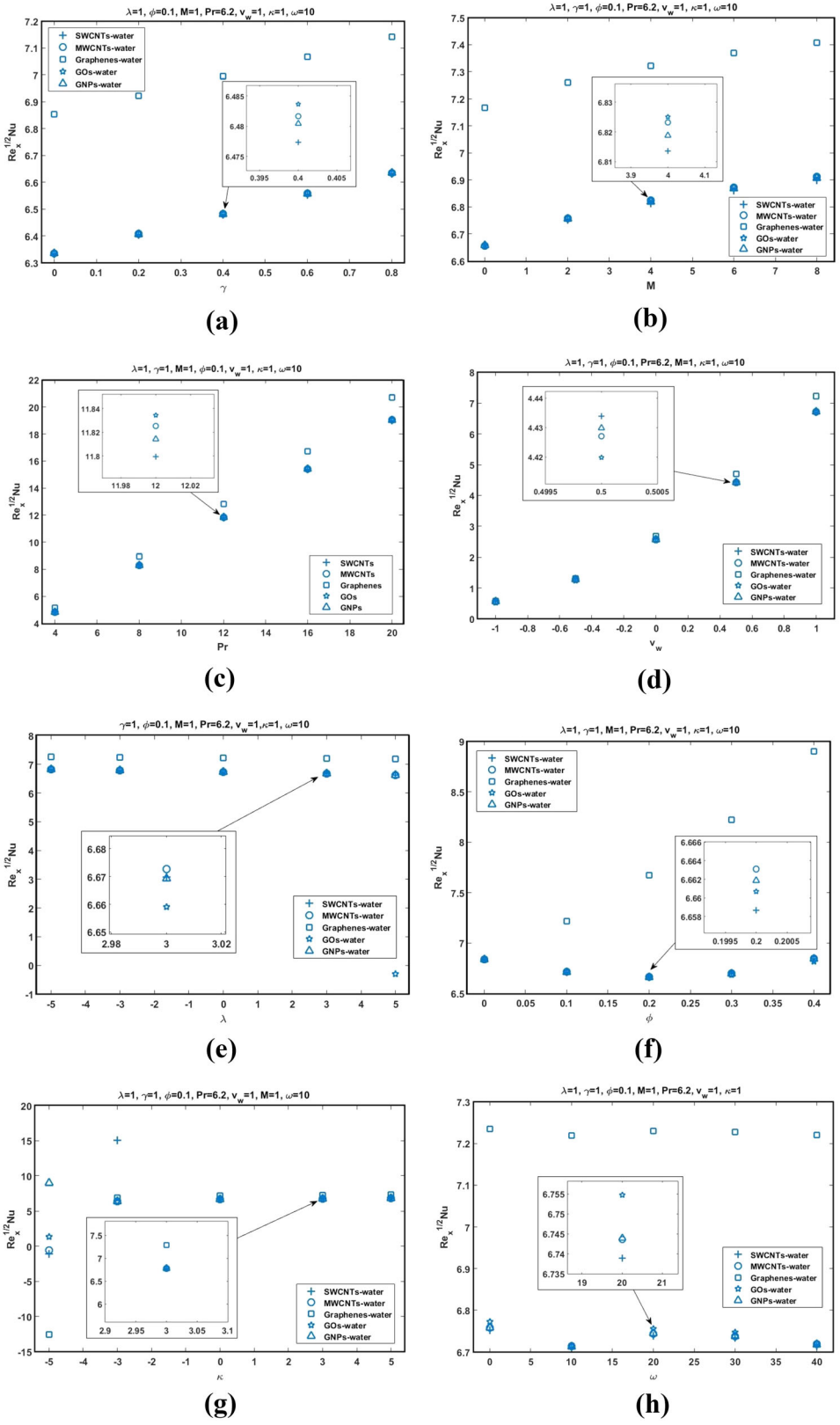

Fig. 8 Impact of parameter variation on reduced Nusselt number for selected nanofluids

Table 3 Impact of parameter variation on reduced skin friction coefficient and Nusselt number for selected nanofluids

λ	γ	ϕ	M	Pr	v_w	κ	ω	$Re^{1/2}C_f$			$Re^{1/2}Nu$		
								Graphene	GOs	GNPs	Graphene	GOs	GNPs
−0.5								3.48962	4.30695	4.10866	7.26165	6.86430	6.83154
−3.0								3.34971	3.82608	3.72324	7.24761	6.81749	6.79381
0.0								3.13819	3.08493	3.13229	7.22611	6.74210	6.73388
3.0								2.92461	2.31578	2.52382	7.20406	6.65914	6.66927
5.0								2.78102	−3.62665	2.10696	7.18904	−0.29992	6.62310
	0.0							2.50492	2.28548	2.38101	6.85475	6.33861	6.33483
	0.2							2.62432	2.40173	2.49791	6.92340	6.40989	6.40640
	0.4							2.73981	2.51402	2.61098	6.99452	6.48364	6.48042
	0.6							2.85186	2.62287	2.72067	7.06770	6.55939	6.55644
	0.8							2.96088	2.72871	2.82741	7.14257	6.63675	6.63404
		0.0						2.52463	2.52463	2.52463	6.83702	6.83702	6.83702
		0.1						3.06723	2.83194	2.93154	7.21882	6.71538	6.71291
		0.2						3.78131	3.20880	3.44517	7.67425	6.66069	6.66186
		0.3						4.75596	3.70906	4.13476	8.22358	6.68608	6.69646
		0.4						6.15781	4.44081	5.13330	8.90219	6.81860	6.84223
			0.0					2.70333	2.44735	2.55738	7.16632	6.65825	6.65847
			2.0					3.37624	3.15492	3.24784	7.25980	6.75918	6.75503
			4.0					3.89602	3.69342	3.77784	7.32239	6.82504	6.81886
			6.0					4.33436	4.14436	4.22334	7.36993	6.87439	6.86697
			8.0					4.72027	4.53968	4.61475	7.40840	6.91399	6.90570
				4.0				3.04433	2.75199	2.86858	5.14408	4.80591	4.81022
				8.0				3.07917	2.87376	2.96457	8.93326	8.28903	8.28096
				12.0				3.09554	2.93145	3.01023	12.80104	11.83432	11.81403
				16.0				3.10503	2.96516	3.03697	16.72804	15.43271	15.40061
				20.0				3.11118	2.98713	3.05441	20.69275	19.06669	19.02310
					−1.0			1.76091	1.30069	1.44835	0.57146	0.52745	0.55736
					−0.5			2.04672	1.64860	1.77896	1.31083	1.24958	1.28017
					0.0			2.36473	2.03420	2.14786	2.68098	2.54812	2.57050
					0.5			2.70661	2.43253	2.53546	4.70681	4.41985	4.42982
					1.0			3.06723	2.83194	2.93154	7.21882	6.71538	6.71291
						−5.0		0.26914	0.06498	1.34659	−12.61173	1.36704	8.97703
						−3.0		1.98242	1.74630	1.83697	6.94523	6.42772	6.42617
						0.0		2.88491	2.64641	2.74749	7.17848	6.67282	6.67116
						3.0		3.36880	3.13959	3.23588	7.28227	6.78216	6.77830
						5.0		3.61687	3.39315	3.48614	7.33181	6.83416	6.82917
							0.0	3.22246	3.38243	3.36900	7.23472	6.77286	6.75820
							10.0	3.06723	3.83194	2.93154	7.21882	6.71538	6.71291
							20.0	3.17262	3.20685	3.22921	7.22963	6.75479	6.74389
							30.0	3.15121	3.13110	3.16898	7.22744	6.74692	6.73768
							40.0	3.08181	2.88410	2.97289	7.22032	6.72093	6.71725

Acknowledgements Contribution of anonymous reviewer/s toward improvement of this work is highly appreciated. The first and the corresponding authors received financial support under the Project RF013B-2018 of Faculty of Science-Universiti Malaya Research Grant (FS-UMRG). We further declare that there is no conflict of interest among the authors on submission and publication process of this manuscript.

References

1. Choi SU, Eastman JA (1995) Enhancing thermal conductivity of fluids with nanoparticles, International mechanical engineering congress and exhibition, San Francisco, CA (United States), 12–17 Nov 1995.https://www.osti.gov/servlets/purl/196525/
2. Haq RU, Nadeem S, Khan ZH, Noor NFM (2015) MHD squeezed flow of water functionalized metallic nanoparticles over a sensor surface. Phys E 73:45–53
3. Pandey AK, Rajput S, Bhattacharyya K, Sibanda P (2021) Impact of metal oxide nanoparticles on unsteady stagnation point flow of the hybrid base fluid along a flat surface. Pramana 95:1–9
4. Sheikholeslami M, Rashidi MM, Ganji DD (2015) Effect of non-uniform magnetic field on forced convection heat transfer of Fe3O4-water nanofluid. Comput Methods Appl Mech Eng 294:299–312
5. Verma AK, Gautam AK, Bhattacharyya K, Sharma RP (2021) Existence of boundary layer nanofluid flow through a divergent channel in porous medium with mass suction/injection. Sadhana 46:1–10
6. Hayat T, Hussain Z, Muhammad T, Alsaedi A (2016) Effects of homogeneous and heterogeneous reactions in flow of nanofluids over a nonlinear stretching surface with variable surface thickness. J Mol Liq 221:1121–1127
7. Bhattacharyya K, Layek GC (2011) Effects of suction/blowing on steady boundary layer stagnation-point flow and heat transfer towards a shrinking sheet with thermal radiation. Int J Heat Mass Transf 54:302–307
8. Seth GS, Singha AK, Mandal MS, Banerjee A, Bhattacharyya K (2017) MHD stagnation-point flow and heat transfer past a non-isothermal shrinking/stretching sheet in porous medium with heat sink or source effect. Int J Mech Sci 134:98–111
9. Kumar PM, Kumar CA (2019) Numerical evaluation of cooling performances of semiconductor using CuO/water nanofluids. Heliyon. https://doi.org/10.1016/j.heliyon.2019.e02227
10. Bhattacharyya K, Mukhopadhyay S, Layek GC (2011) Slip effects on boundary layer stagnation-point flow and heat transfer towards a shrinking sheet. Int J Heat Mass Transf 54:308–313
11. Selimefendigil F, Öztop HF (2019) MHD mixed convection of nanofluid in a flexible walled inclined lid-driven L-shaped cavity under the effect of internal heat generation. Statist Mech Appl, Phys A, p 122144. https://doi.org/10.1016/j.physa.2019.122144
12. Dinarvand S, Hosseini R, Pop I (2017) Axisymmetric mixed convective stagnation-point flow of a nanofluid over a vertical permeable cylinder by Tiwari-Das nanofluid model. Powder Technol 311:147–156
13. Gholinia M, Gholinia S, Hosseinzadeh K, Ganji DD (2018) Investigation on ethylene glycol nano fluid flow over a vertical permeable circular cylinder under effect of magnetic field. Results Phys 9:1525–1533
14. Reddy SRR, Reddy PBA, Bhattacharyya K (2019) Effect of nonlinear thermal radiation on 3D magneto slip flow of Eyring-Powell nanofluid flow over a slendering sheet with binary chemical reaction and Arrhenius activation energy. Adv Powder Technol 30:3203–3213
15. Ashorynejad HR, Zarghami A (2018) Magnetohydrodynamics flow and heat transfer of Cu-water nanofluid through a partially porous wavy channel. Int J Heat Mass Transf 119:247–258
16. Purbia D, Khandelwal A, Kumar A, Sharma AK (2019) Graphene-water nanofluid in heat exchanger: mathematical modelling, simulation and economic evaluation. Int Commun Heat Mass Transf. https://doi.org/10.1016/j.icheatmasstransfer.2019.104327
17. Sheikholeslami M, Shamlooei M, Moradi RJCE (2018) Numerical simulation for heat transfer intensification of nanofluid in a porous curved enclosure considering shape effect of Fe3O4 nanoparticles. Chem Eng Process-Process Intensif 124:71–82
18. Haq RU, Nadeem S, Khan ZH, Noor NFM (2015) Convective heat transfer in MHD slip flow over a stretching surface in the presence of carbon nanotubes. Phys B 457:40–47
19. Kumar V, Tiwari AK, Ghosh SK (2015) Application of nanofluids in plate heat exchanger: a review. Energy Convers Manage 105:1017–1036
20. Sadeghinezhad E, Mehrali M, Saidur R, Mehrali M, Latibari ST, Akhiani AR, Metselaar HSC (2016) A comprehensive review on graphene nanofluids: recent research, development and applications. Energy Convers Manage 111:466–487
21. Ghozatloo A, Rashidi A, Shariaty-Niassar M (2014) Convective heat transfer enhancement of graphene nanofluids in shell and tube heat exchanger. Exp Thermal Fluid Sci 53:136–141
22. Tiwari RK, Das MK (2007) Heat transfer augmentation in a two-sided lid-driven differentially heated square cavity utilizing nanofluids. Int J Heat Mass Transf 50(9–10):2002–2018
23. Oztop HF, Abu-Nada E (2008) Numerical study of natural convection in partially heated rectangular enclosures filled with nanofluids. Int J Heat Fluid Flow 29(5):1326–1336
24. Muhammad S, Ali G, Shah Z, Islam S, Hussain S (2018) The rotating flow of magneto hydrodynamic carbon nanotubes over a stretching sheet with the impact of non-linear thermal radiation and heat generation/absorption. Appl Sci. https://doi.org/10.3390/app8040482
25. Sandeep N, Malvandi A (2016) Enhanced heat transfer in liquid thin film flow of non-Newtonian nanofluids embedded with graphene nanoparticles. Adv Powder Technol 27(6):2448–2456
26. Upadhya SM, Raju CSK, Saleem S, Alderremy AA (2018) Modified Fourier heat flux on MHD flow over stretched cylinder filled with dust, graphene and silver nanoparticles. Results Phys 9:1377–1385
27. Javanmard M, Taheri MH, Abbasi M, Ebrahimi SM (2018) Heat transfer analysis of hydromagnetic water-graphene oxide nanofluid flow in the channel with asymmetric forced convection on walls. Chem Eng Res Des 136:816–824
28. Azimi M, Azimi A, Mirzaei M (2014) Investigation of the unsteady graphene oxide nanofluid flow between two moving plates. J Comput Theor Nanosci 11(10):2104–2108
29. Amin M, Putra N, Kosasih EA, Prawiro E, Luanto RA, Mahlia TMI (2017) Thermal properties of beeswax/graphene phase change material as energy storage for building applications. Appl Therm Eng 112:273–280